

Global Deterministic Optimization with Artificial Neural Networks Embedded

Artur M. Schweidtmann and Alexander Mitsos

RWTH Aachen University

AVT - Aachener Verfahrenstechnik

Process Systems Engineering

Forckenbeckstr. 51

D - 52074 Aachen

This is a pre-print of an article published in *Journal of Optimization Theory and Applications*. The final authenticated version is available online at: <https://doi.org/10.1007/s10957-018-1396-0>.

1 Abstract

Artificial neural networks (ANNs) are used in various applications for data-driven black-box modeling and subsequent optimization. Herein, we present an efficient method for deterministic global optimization of ANN embedded optimization problems. The proposed method is based on relaxations of algorithms using McCormick relaxations in a reduced-space [*SIOPT*, 20 (2009), pp. 573-601] including the convex and concave envelopes of the nonlinear activation function of ANNs. The optimization problem is solved using our in-house global deterministic solver MAiNGO. The performance of the proposed method is shown in four optimization examples: an illustrative function, a fermentation process, a compressor plant and a chemical process optimization. The results show that computational solution time is favorable compared to the global general-purpose optimization solver BARON.

Keywords: Surrogate-based optimization, Multilayer perceptron, McCormick relaxations, Machine learning, Deep learning, Fermentation process, Compressor plant, Cumene process

AMS subject classification: 90C26, 90C30, 90C90, 68T01

2 Introduction

A feed-forward ANN with one hidden layer can approximate any smooth function on a compact domain to an arbitrary degree of accuracy given a sufficient number of neurons [1]. Thus, artificial neural networks (ANNs) are said to be universal approximators. Due to their excellent approximation properties, ANNs have attracted widespread interest in various fields such as chemistry [2], chemical engineering [3], pharmaceutical research [4] and biosorption processes [5] for the black-box modeling of complex systems. Furthermore, various industry applications of ANNs exist, e.g., modeling and identification, optimization

and process control [6].

In many of these applications, a model including ANNs is developed and then used for optimization. In biochemical engineering for example, ANNs are commonly used to model fermentation processes [7] and optimize their output to identify promising operating points for further experiments [8–10]. ANNs are also used as surrogate models for the optimization of chemical processes [11–24].

Most of the previous optimizations with ANNs embedded rely on local optimization techniques. Fernandes, for instance, optimized the product concentrations of a Fischer-Tropsch synthesis using the quasi-Newton method and finite-differences [25]. Other authors used local solvers like DICOPT [26] (e.g., [11, 15, 16, 19]), sequential quadratic programming (e.g., [17]) or CONOPT [27] (e.g., [19]). These local methods can yield suboptimal solutions when the learned input-output relation is multi-modal. In addition, the activations functions involved in ANNs are usually nonconvex. A few researchers have addressed this problem by using stochastic global methods such as genetic algorithms (e.g., [8–10, 22, 23, 28]) or brute-force grid search (e.g., [12–14]). These methods cannot guarantee global optimality. Global deterministic optimization of an ANN embedded problem was done by Smith *et al.* (2013) [18] who used BARON [29–31] to optimize an ANN with one hidden layer and three neurons that emulates a flooded bed algae bioreactor. As the hyperbolic tangent activation function is currently not available in BARON, Smith *et al.* reformulated the activation function using exponential functions. Henao argues in his Ph.D. thesis [19] that state-of-the-art global optimization solvers such as BARON are at that time, i.e., 2012 limited to small to medium sized problems and he suggests a piecewise linear approximation of the hyperbolic tangent function. The literature shows that there remains a need for an efficient deterministic global optimization algorithm of problems with ANNs embedded.

There have been many other efforts to combine surrogate modeling with (global) optimization. For instance, Gaussian processes (GPs) have been used in the field of Bayesian optimization for optimization of expensive-to-evaluate

black-box functions (e.g., [32–36]). In the adaptive approach, GPs emulate black-box objectives, e.g., measurements of a chemical experiment [37], in every iteration to assist a following query point selection. ALAMO is another adaptive sampling approach [38–40] that aims the development of simple surrogate models in the light of small data sets. This contribution focuses on the development of a global deterministic optimization approach for problems including (given) well-established ANN surrogate models. In contrast to standard GPs, ANNs can have multiple outputs and can handle large training sets (i.e., GP training requires N by N matrix inversions where N is the number of training points).

In deterministic global optimization, convex relaxations are derived and relaxed problems are solved using branch-and-bound (B&B) [41, 42] or related algorithms [29–31, 43]. In most state-of-the-art deterministic global optimization solvers such as BARON [29–31], ANTIGONE [43] and SCIP [44] the complete set of constraints and variables is handed to the optimization algorithm that builds convex relaxations. This method is referred to as the full-space (FS) formulation. Another possibility is the reduced-space (RS) formulation. The key idea herein is that the optimizer does not see all variables and constraints [45–49].

For the deterministic global optimization of ANNs, the FS inherently results in a large-scale optimization problem because the ANN network structure includes multiple (hidden) layers, neurons and network equations. Additionally, auxiliary variables used in state-of-the-art solvers for the relaxations increase the problem size. Globally solving large-scale optimization problems is difficult because of the exponential worst-case runtime of the B&B algorithm. Moreover, in standard solvers the user has to provide tight variable bounds which are difficult to provide for some network variables. A possible disadvantage of the RS formulation is that the propagation of relaxations through large ANNs may result in weak relaxations.

One possibility to construct relaxations in the RS setup are McCormick re-

laxations [50, 51] that have shown favorable convergence properties [52, 53] and have been extended to the relaxation of multivariate functions [54] and bounded functions with discontinuities [55]. Recently, a differentiable modification of the relaxations has been proposed as well [56]. The global optimization using McCormick relaxations has been applied to several problems such as flowsheet optimization [48, 49, 57] and the solution of ODE and nonlinear equation systems [47, 58, 59]. Besides the direct utilization of McCormick relaxations in the original variables, the method was also used in the development of the auxiliary variable method (AVM) that is applied in state-of-the-art solvers [43, 60, 61].

In this contribution, ANNs are optimized in a RS which significantly reduces the dimensionality of the optimization problems. More specifically, the equations that describe the ANN and the corresponding variables are hidden from the B&B solver. In order to construct tight convex and concave relaxations of the ANNs, we utilize the convex and concave envelopes of the activation function (shown in Appendix A.1) and automatic construction of McCormick relaxations [46].

In the remainder of this paper, first an overview about multilayer perceptron ANNs is provided (Section 3). In Section 4, the optimization problem formulation and the relaxation of ANNs are proposed. Further, implementation details are provided. In Section 5, the proposed method is applied to four numerical examples illustrating its potential and compared to a state-of-the-art general purpose optimization algorithm BARON in terms of computational (CPU) time. In Section 6, advantages, limitations and prospective utility of the proposed method are discussed.

3 Background on Multilayer Perceptrons

In this subsection, the multilayer perceptron (MLP), also known as feed-forward ANN, is briefly introduced. More detailed information about MLPs can be found in the literature (e.g., [62]). As depicted in Figure 1, the MLP can be illustrated

as a directed acyclic graph connecting multiple layers, k , of neurons, which are the nodes of the graph. It consists of an input layer ($k = 1$), a number of hidden layers ($k = 2, \dots, N - 1$) and an output layer ($k = N$). Each connection between a neuron j of layer k and neuron i of layer $k + 1$ is associated with a weight $w_{j,i}^{(k)}$. The output, $z_i^{(k+1)}$, of a neuron i in layer k is given by

$$z_i^{(k+1)} = h_{k+1} \left(\sum_{j=1}^{D^{(k)}} (w_{j,i}^{(k)} z_j^{(k)}) + w_{0,i}^{(k)} \right) \quad (1)$$

where $h_k : \mathbb{R} \rightarrow \mathbb{R}$ is the activation function, $D^{(k)}$ is the number of neurons in each layer and $w_{0,i}^{(k)}$ is a bias parameter. Thus, the argument of h is a linear combination of the outputs of the previous layer. The output value of neurons in the input layer ($z_i^{(1)}$) correspond to the network input variables. Following (1) for all neurons and layers, the outputs (also called predictions) of the network ($z_i^{(N)}$) can be computed.

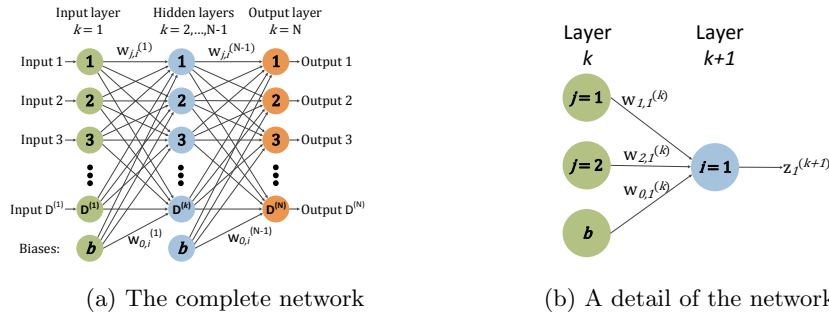


Fig. 1: Graphical illustration of a multilayer perceptron artificial neural network as a directed acyclic graph

A commonly-used activation function of the hidden layers is the hyperbolic tangent function ($h_k(x) = \tanh(x)$). In the output layer, the identity activation function ($h_N(x) = x$) is typically used for regression problems. Thus, this work focuses on the hyperbolic tangent function. However, the proposed method can be easily applied to other common activation functions like the sigmoid function (see Appendix A.2).

4 Method

In this section, the optimization problem formulations and the McCormick relaxation of MLPs are proposed. Further, details about the implementation are provided.

4.1 Optimization Problem Formulations

Optimization problems which use MLPs as surrogate models often have a particular structure. Usually, one or more of the input variables, \mathbf{x} , correspond to degrees of freedom of the problem and can be chosen within given bounds $D = [\mathbf{x}^L, \mathbf{x}^U]$. Once the input variables are fixed, the dependent variables in the networks, \mathbf{z} , can be determined by solving the nonlinear network equations $\mathbf{h}(\mathbf{x}, \mathbf{z}) = \mathbf{0}$, $\mathbf{h} : D \times \mathbb{R}^{n_z} \rightarrow \mathbb{R}^{n_z}$. The nonlinear network equations of MLPs can also be formulated explicitly in the outputs as shown in Subsection 4.1.2. The outputs \mathbf{y} of the networks can be understood as network variables of the output layers. Thus, the output variables are a subset of the network variables with $n_y < n_z$. The objective function, $f(\mathbf{x}, \mathbf{y})$, $f : D \times \mathbb{R}^{n_y} \rightarrow \mathbb{R}$, usually depends on the networks inputs and outputs but not on the remaining network variables. Similarly, the feasible region is often constrained by inequalities $\mathbf{g}(\mathbf{x}, \mathbf{y}) \leq \mathbf{0}$, $\mathbf{g} : D \times \mathbb{R}^{n_y} \rightarrow \mathbb{R}^{n_g}$ which also depend only on the network inputs and outputs.

4.1.1 Full-space formulation

In the FS formulation, the input and the network variables are optimization variables and the problem can be formulated as follows:

$$\begin{aligned} & \min_{\mathbf{x} \in D, \mathbf{z} \in Z} && f(\mathbf{x}, \mathbf{y}) \\ & \text{s.t.} && \mathbf{h}(\mathbf{x}, \mathbf{z}) = \mathbf{0} \\ & && \mathbf{g}(\mathbf{x}, \mathbf{y}) \leq \mathbf{0} \end{aligned} \quad (\text{FS})$$

In this case, a global B&B solver requires bounds on \mathbf{x} and \mathbf{z} . As mentioned in the introduction, the FS formulation is utilized by common general-purpose deterministic global optimization solvers.

4.1.2 Reduced-space formulation

In MLPs the network equations $\mathbf{h}(\mathbf{x}, \mathbf{z}) = \mathbf{0}$ can be reformulated as an explicit function $\hat{\mathbf{y}} : D \rightarrow \mathbb{R}^{n_y}$ with $\mathbf{y} = \hat{\mathbf{y}}(\mathbf{x})$. Thus, the dependent network variables can be eliminated from the FS optimization formulation (c.f. [48]). The resulting optimization problem can be formulated as follows:

$$\begin{aligned} \min_{\mathbf{x} \in D} \quad & f(\mathbf{x}, \hat{\mathbf{y}}(\mathbf{x})) && \text{(RS)} \\ \text{s.t.} \quad & \mathbf{g}(\mathbf{x}, \hat{\mathbf{y}}(\mathbf{x})) \leq \mathbf{0} \end{aligned}$$

The RS formulation operates only in the domain D of the optimization variables x . Further, the equality constraints which describe the network equations are not visible to the optimization algorithm anymore. However, it is important to note that the complete elimination of equality constraints is not necessarily possible when optimizing arrangements of several MLPs or hybrid modeling formulations. In these cases, some equality constraints and additional variables might remain in the RS formulation (e.g., for connecting different MLPs with a recycle) similar to, e.g., [48]. As an option, these can also be relaxed using extensions of the McCormick approach to implicit functions [58, 59].

4.2 Relaxations of Artificial Neural Networks

In order to solve the RS optimization problem using the B&B algorithm, lower-bounds of the MLPs have to be derived. In this paper, the lower bounds are calculated by automatic propagation of McCormick relaxations and natural interval extensions [63, 64] using the open-source software MC++ [65, 66] (see Section 4.3). As described in Section 3, the outputs of MLPs are compositions of the activation functions and affine functions that connect the neurons. Thus,

the only nonlinearities of MLPs are its activation functions. When using MLPs as a surrogate model, the hyperbolic tangent function (\tanh) is commonly used as the activation function in the hidden layers and the identity is usually used as the activation function in the output layer [62]. Thus, the tightness of MLP relaxations is considerably influenced by the relaxations of the hyperbolic tangent function.

In general, McCormick relaxations do not provide the envelopes (tightest possible relaxations). The envelopes of the hyperbolic tangent function are derived in Appendix A.1. They are once continuously differentiable (Proposition A.1) and strictly monotonically increasing (Proposition A.3).

In the proposed framework, the envelopes of the hyperbolic tangent activation function are propagated through the network equations to derive concave and convex relaxations of the outputs of MLPs. The resulting relaxations of MLPs are once continuously differentiable as shown in the following proposition.

Proposition 4.1 (*smoothness of MLP relaxations*). *Consider an MLP using (exclusively) the hyperbolic and identity activation functions. The McCormick relaxations built with the envelopes of the hyperbolic tangent function (Appendix A.1) are once continuously differentiable.*

Proof Consider the output of a neuron in a hidden layer as a function of its inputs. As the convex and concave relaxations of the hyperbolic tangent activation function are monotonically increasing (see Proposition A.3), Corollary 3 by [54] holds. Thus, the convex and concave relaxation of the output of the neuron are compositions of the corresponding relaxation of the hyperbolic tangent function and the corresponding relaxations of the inputs to the neuron. As the envelopes of the hyperbolic tangent function are once continuous differentiable (see Proposition A.1), the relaxations of the MLPs are once continuous differentiable by chain rule. \square It should be noted that the relaxations are not C^2 because the envelopes of the hyperbolic tangent function are not C^2

(see Proposition A.1). However, Proposition A.2 shows that the first derivative of the convex and concave envelopes of the hyperbolic tangent function, $\frac{d(F^{cv})}{dx}$ and $\frac{d(F^{cc})}{dx}$, are Lipschitz continuous (sometimes referred to as $C^{1,1}$). Recall that we use the hyperbolic tangent function because it is the most commonly used and similar results can be derived for other activation functions.

Proposition 4.1 has a beneficial consequence for the global optimization of MLPs. In general, McCormick relaxations are continuous but not differentiable (C^0). This necessitates nonsmooth algorithms, e.g., bundle methods [67, 68] or linearization-based methods [46]. However, when optimizing MLPs, a $C^{1,1}$ optimization algorithm can be used which is potentially more efficient.

In the general-purpose optimization solvers BARON, ANTIGONE and SCIP, the hyperbolic tangent function is currently not available and interfaces do not allow the user to define functions and/or relaxations. In order to compare the performance of the proposed method to these algorithms, the hyperbolic tangent activation function can be reformulated. As the tightness of the McCormick relaxations of different reformulations can differ, the relaxations of four common reformulations $F_1, F_2, F_3, F_4 : \mathbb{R} \rightarrow \mathbb{R}$ with $F_1(x) := \frac{e^x - e^{-x}}{e^x + e^{-x}}$, $F_2(x) := \frac{e^{2x} - 1}{e^{2x} + 1}$, $F_3(x) := 1 - \frac{2}{e^{2x} + 1}$, $F_4(x) := \frac{1 - e^{-2x}}{1 + e^{-2x}}$ are compared in Appendix A.3. The exemplary plot of the McCormick relaxations in the appendix shows that the convex and concave relaxations of F_1, F_2 and F_4 are weaker than the ones of F_3 . Further, the convex and concave relaxations of F_1, F_2 and F_4 are not differentiable. Finally, it can be observed that relaxations of the reformulations are considerably weaker than the envelopes.

4.3 Implementation

The proposed work uses the in-house McCormick based Algorithm for mixed integer Nonlinear Global Optimization (MAiNGO), a B&B optimization solver in C++ [69]. Herein, a best-first heuristic and bisection along the longest edge is used for branching. For lower bounding, a convex underestimation of the problem is found by automatic propagation of McCormick relaxations using the

open-source software MC++ v2.0 [65, 66]. The necessary interval extensions are provided by FILIB++ v3.0.2 [64]. The convex relaxations of the constraints and the objective are linearized with the use of subgradients at the centerpoint of each node and the resulting linear program (LP) is solved by CPLEX v12.5 [70]. Further, optimization-based bound tightening is used that is improved by filtering bounds technique with a factor of 0.1 as described in [71] and bound tightening based on the dual multipliers returned by CPLEX is used [72, 73]. For upper bounding, the problem is locally optimized using the SLSQP algorithm [74, 75] in the NLOpt library v2.4.2 [76]. The necessary derivatives are provided by the FADBAD++ tool for automatic differentiation [77]. Furthermore, recently developed heuristics for tighter McCormick relaxations are used [78].

The convex and concave envelopes of \tanh are added to the MC++ library. In order to compute those envelopes, the equations (8) and (10) have to be solved numerically (see Appendix A.1). For this purpose, the Newton method is used and analytical gradient information is supplied.

The ANNs in this work are fitted in the Neural Network Toolbox in MATLAB.

5 Numerical Results

In this section, the numerical results of four case studies are presented. The performance of the proposed method is compared to the general-purpose optimization solver BARON 17.4.1. using GAMS 24.8.5. All numerical examples were run on one thread of an Intel Xeon CPU E5-2630 v2 with 2.6 GHz, 128 GB RAM and Windows Server 2008 operating system.

5.1 Illustrative Example & Scaling of the Algorithm

In the first illustrative example, a two-dimensional mathematical test function is learned by a MLP that is subsequently optimized. The peaks function is

provided by Matlab (*peaks()*) and is given by $f_{peaks} : \mathbb{R}^2 \rightarrow \mathbb{R}$ with

$$f_{peaks}(x_1, x_2) = 3(1-x_1)^2 \cdot e^{-x_1^2 - (x_2+1)^2} - 10 \cdot \left(\frac{x_1}{5} - x_1^3 - x_2^5\right) \cdot e^{-x_1^2 - x_2^2} - \frac{e^{-(x_1+1)^2 - x_2^2}}{3} \quad (2)$$

The function has multiple local optima on $D = \{x_1, x_2 \mid -3 \leq x_1, x_2 \leq 3\}$.

The known unique global minimizer of the test function is $\min_{x_1, x_2 \in D} f_{peaks}(x_1, x_2) = -6.551$ at $(x_1^*, x_2^*) = (0.228, -1.626)$.

To learn the peaks function, a Latin hypercube (LHC) sampling technique is used to generate a set of 500 points on D . As mentioned in the introduction, a MLP with one hidden layer is a universal approximator. Thus, a network architecture with one hidden layer is chosen in this example. The MLP constitutes two neurons in the input layer and one neuron in the output layer. In order to avoid over- and under-fitting, D is randomly divided into a training, a validation and a test sets with the respective size ratios of 0.7 : 0.15 : 0.15. The weights of the network are fitted in the Matlab Neural Network Toolbox by minimizing the mean squared error (MSE) on the training set using Levenberg-Marquardt algorithm and the early stopping procedure [62]. To obtain a suitable number of neurons in the hidden layer the training is repeated using different number of neurons. The configuration with the lowest MSE on the test set determines the number of neurons to be 47. The training results in a MSE of $6.8 \cdot 10^{-5}$, $3.9 \cdot 10^{-4}$ and $4.6 \cdot 10^{-4}$ on the training, validation and test set respectively.

After training, the MLP is optimized using the proposed methods. The absolute optimization tolerance is set to $\epsilon_{tol} = 10^{-4}$ because more accurate solution of the optimization problem is not sensible due to the prediction error of the MLP. The relative tolerance is set to its minimum value (10^{-12}) and is thus not active. This way the optimization result is limited by the prediction accuracy only. Further, a time limit of 100,000 seconds (about 28 hours) is set for the optimization.

Table 1 summarizes the results of the optimization runs. The results show that the problem formulation has a significant influence on the problem size.

In comparison to the FS formulations, the RS formulation reduces the number of the optimization variable from 101 to 2 and eliminates all 99 equality constraints. The RS formulation requires over 190 times less CPU time compared to the FS formulation when using the presented solver. Further, different relaxations of the activation function yield different solution times. The envelope of the activation function accelerates the optimization significantly compared to all reformulations. When the presented solver is used in the FS formulation, the weak relaxations of the reformulations even lead to a variable overflow error in the exponential function in FILIB++. As expected from the comparison of the relaxations (see Appendix A.3), reformulation F_3 outperforms the other reformulations in terms of computational efficiency. In general, all RS optimizations converged to the same optimal solution (-6.563). The solution is about 0.18% different from the global optimizer of the underlying peaks function. This is within the expected accuracy of the MLP prediction.

Table 1: Numerical results of the peaks function optimization (Subsection 5.1)

	Problem size	Solver	CPU time [s]	Iterations	Abs. gap
(FS)	101 variables	BARON (F_1)	1,727.29	55,047	$< \epsilon_{\text{tol}}$
	99 equalities	BARON (F_2)	387.44	13,329	$< \epsilon_{\text{tol}}$
	0 inequalities	BARON (F_3)	21.08	1,223	$< \epsilon_{\text{tol}}$
		BARON (F_4)	100,000.00	2,732,488	0.0003
		Presented solver (F_1)	-variable overflow-		
		Presented solver (F_2)	-variable overflow-		
		Presented solver (F_3)	-variable overflow-		
		Presented solver (F_4)	-variable overflow-		
		Presented solver (envelope)	84.19	1	$< \epsilon_{\text{tol}}$
	(RS)	2 variables	Presented solver (F_1)	18.61	8,825
0 equalities		Presented solver (F_2)	23.06	17,785	$< \epsilon_{\text{tol}}$
0 inequalities		Presented solver (F_3)	0.73	933	$< \epsilon_{\text{tol}}$
		Presented solver (F_4)	10.50	11,857	$< \epsilon_{\text{tol}}$
		Presented solver (envelope)	0.44	207	$< \epsilon_{\text{tol}}$

variable overflow: Crashed due to variable overflow in FILIB++.

In a second step, the peaks function is used to illustrate the scaling of the optimization algorithm with network size. Therefore, networks with different sizes are trained on a LHC set of 2,000 points. Subsequently, the networks are optimized. In Subfigure 2 (a), the number of neurons in the hidden layer of a shallow MLP is varied from 40 to 700 and the computational time for optimization is depicted. The RS formulation using the envelope and the reformulation

F_3 shows a consistent increase of CPU time with the number of neurons whereas the CPU time of BARON using F_3 does not show a clear trend. For instance, BARON did not converge within 100,000 seconds for networks with 60, 80, 240, 260 and 340 neurons but shows good performance for a network with 700 neurons. The optimization using the FS formulation and the presented solver shows the weakest performance. As most of these optimizations with more than 100 neurons did not converge within 100,000 seconds, this optimization was not executed for networks with more than 100 neurons. The presented solver using the RS formulation and the envelope shows consistently one of the best performances. It should be noted that the number of neurons is unreasonable high for this illustration which leads to overfitting. It can further be noted that the network sizes (up to 700 neurons) exceed the network size of the case study by Smith *et al.* (2013) [18] (3 neurons) drastically.

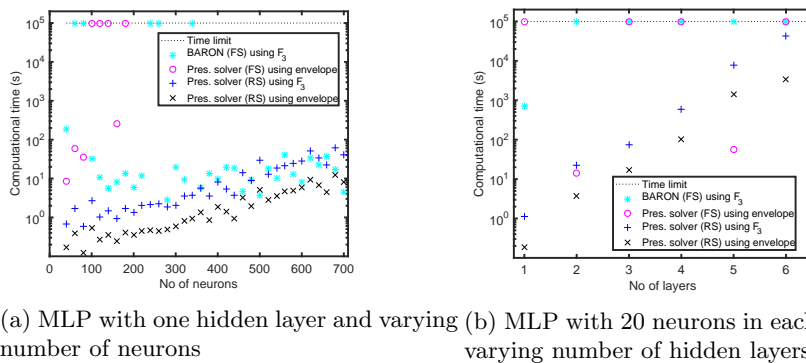


Fig. 2: Graphical illustration of the computational time over the ANN size for the peaks function optimization problem (Subsection 5.1)

In Subfigure 2 (b), the number of neurons in each hidden layer is fixed to 20 and the number of hidden layers is varied from 1 to 6. The results show that the CPU times of the presented solver using the RS formulation increases approximately exponentially with the number of layers. Further, the utilization of the envelopes has always an advantage over the reformulation F_3 . The solution of the FS formulation using either BARON or the presented solver does not converge to an optimal solution within the time limit for most cases. In general,

it is apparent that deep networks require more CPU time for optimization than shallow networks with the same or even larger number of neurons.

5.2 Fermentation Process

In the second subsection, a fermentation of glucose to gluconic acid is learned from experimental data and optimized. The example is based on and compared to the work of Cheema *et al.* [8] where an MLP is learned from experimental data and optimized using stochastic optimization approaches. The numerical example is relevant because mechanistic models of fermentation processes are often not available and surrogate-based optimization can help to identify promising operating conditions.

The inputs of the MLP and degrees of freedom are the glucose concentration (x_1 in [g/L]), the biomass concentration (x_2 in [g/L]) and the dissolved oxygen (x_3 in [mg/L]), whereas the output of the MLP is the concentration of gluconic acid (y in [g/L]). The objective of the optimization problem is to maximize the yield of gluconic acid defined as $y_{gl} = \frac{100y}{1.088x_1}$. As the network weights used by Cheema *et al.* [8] are not available, we trained a MLP using the same structure, training and validation data, and training algorithm.

After the training, we performed deterministic global optimization to maximize the gluconic acid yield. The result of the global deterministic optimization is $x_1 = 156.466$ g/L, $x_2 = 3$ g/L, $x_3 = 57.086$ mg/L, $y = 170.127$ g/L and $y_{gl} = 99.937$ which is similar to the literature result. However, it is important to note that the underlying network is rebuild based on the data and it is very unlikely that the network is identical to the one from literature. The main difference to the results from literature is that all deterministic methods in this work converge to the same solution whereas the stochastic literature method shows considerable variations in their solutions, i.e., even the top three out of hundreds of executions of the genetic algorithm (GA) and the simultaneous perturbation stochastic approximation (SPSA) show variations [8].

Due to the small network size, the problem size of the RS is only slightly

smaller than the FS formulation (compare Table 2). The CPU time of the presented solver using the envelope and RS formulation is about 5.4 times faster than the FS formulation. Thus, the RS formulation is favorable with a CPU time of 0.11 seconds. Again, different reformulation of the activation function yield different CPU times. In particular, the CPU time of reformulations F_1 and F_2 in the RS are a unexpectedly large. When considering only reformulations F_1 and F_2 , BARON converges significantly faster to an optimal solution. Further, the CPU time of BARON using different reformulations does not seem to directly relate to the tightness of their McCormick relaxations.

Table 2: Numerical results of the fermentation process optimization (Subsection 5.2)

	Problem size	Solver	CPU time [s]	Iterations	Abs. gap
(FS)	13 variables	BARON (F_1)	14.38	8,233	$< \epsilon_{\text{tol}}$
	10 equalities	BARON (F_2)	0.44	5	$< \epsilon_{\text{tol}}$
	0 inequalities	BARON (F_3)	0.56	7	$< \epsilon_{\text{tol}}$
		BARON (F_4)	0.48	15	$< \epsilon_{\text{tol}}$
		Presented solver (F_1)		–variable overflow–	
		Presented solver (F_2)		–variable overflow–	
		Presented solver (F_3)		–variable overflow–	
		Presented solver (F_4)		–variable overflow–	
		Presented solver (envelope)	0.59	157	$< \epsilon_{\text{tol}}$
	(RS)	3 variables	Presented solver (F_1)	1,100.43	60,752,735
0 equalities		Presented solver (F_2)	13,969.50	49,267,409	$< \epsilon_{\text{tol}}$
0 inequalities		Presented solver (F_3)	0.91	789	$< \epsilon_{\text{tol}}$
		Presented solver (F_4)	11.50	11,021	$< \epsilon_{\text{tol}}$
		Presented solver (envelope)	0.11	57	$< \epsilon_{\text{tol}}$

variable overflow: Crashed due to variable overflow in FILIB++.

5.3 Compressor Plant

In the third numerical example, the operating point of a compressor plant is optimized. This is a relevant case study because air compressors are commonly used in industry and have a high electrical power consumption, e.g., in cryogenic air separation units. In addition, the power consumption of industrial compressors is often provided in form of data (compressor maps, e.g., Figure 4) and not mechanistic models preventing model-based optimization techniques. The considered compressor plant is comprised of two compressors that are connected in parallel as shown in Figure 3. The compressors are sized such that a large

compressor (compressor 1) is supplemented by a smaller compressor (compressor 2). The intent is to minimize the electrical power consumption of the overall process by optimal operation. Mathematically, the case study is challenging as it combines two MLPs with two hidden layers in one optimization problem.

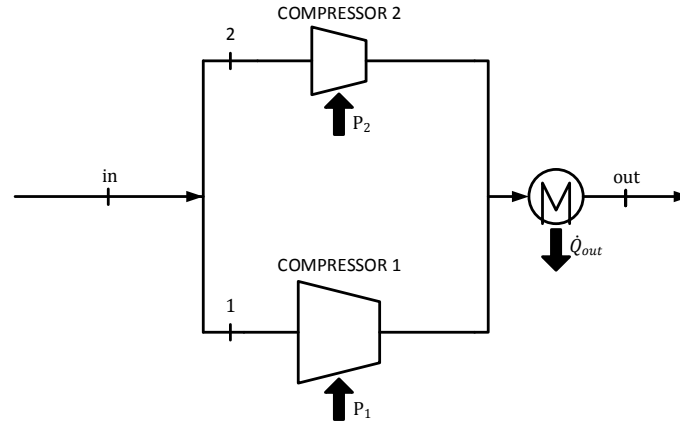


Fig. 3: Graphical illustration of the compressor configuration

The specific power of the compressors is given by compressor maps $M_i : \mathbb{R}^2 \rightarrow \mathbb{R}$ (Figure 4) that map the volumetric inlet flow rate, \dot{V}_i , and compression ratio, $\Pi_i = \frac{p_{out,i}}{p_{in,i}}$, to the specific power, w_i , of the corresponding compressor i (maps were altered from industrial compressor maps). For the MLP training, a set of 405 data points is read out from each compressor map and randomly divided into a training, validation and test set with the respective size ratios of 0.7 : 0.15 : 0.15. Ghorbanian and Gholamrezaei compared different regression models for compressor performance prediction and concluded that the MLP is the most powerful candidate [79]. Thus, this numerical example utilizes the network structure suggested by Ghorbanian and Gholamrezaei, namely a MLP with two hidden layers with 10 neurons each. For training, Levenberg-Marquardt algorithm and early stopping were used on a scaled training data set. The training results in a MSE of 0.17 (0.95), 0.78 (3.87) and 0.39 (1.67) on the training, validation and test set respectively for compressor one (two).

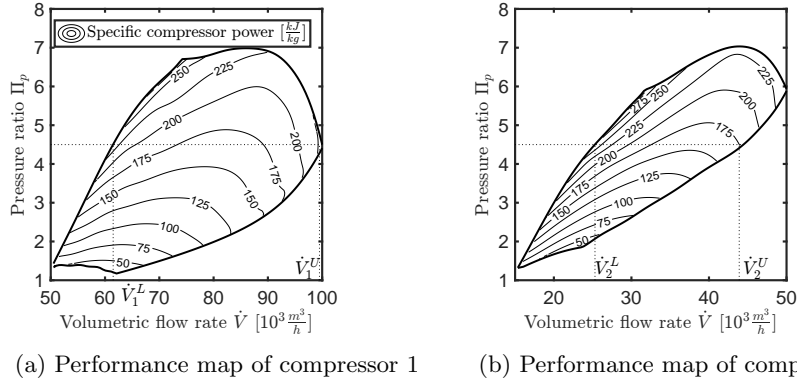


Fig. 4: Graphical illustration of the compressors' specific performance maps

The optimization problem minimizes the total power consumption of the compressor plant, P_{total} . It has one degree of freedom, the split factor (x), that determines the ratio between the volumetric flow rate \dot{V}_1 and the total volumetric inlet flow rate, \dot{V}_{in} . The problem is formulated as follows:

$$\begin{aligned}
 \min_{0 \leq x \leq 1} \quad & P_{\text{total}}(x) = w_{1,\text{MLP}}(\Pi_p, \dot{V}_1) \cdot \frac{\dot{V}_{\text{in}} \cdot x}{v_{\text{in}}} + w_{2,\text{MLP}}(\Pi_p, \dot{V}_2) \cdot \frac{\dot{V}_{\text{in}} \cdot (1-x)}{v_{\text{in}}} \\
 \text{s.t.} \quad & \dot{V}_1 - \dot{V}_1^U \leq 0 \\
 & \dot{V}_1^L - \dot{V}_1 \leq 0 \\
 & \dot{V}_2 - \dot{V}_2^U \leq 0 \\
 & \dot{V}_2^L - \dot{V}_2 \leq 0
 \end{aligned} \tag{3}$$

with the constants $v_{\text{in}} = 0.8305 \frac{\text{m}^3}{\text{kg}}$, $p_{\text{in}} = 100 \text{ kPa}$, $p_{\text{out}} = 450 \text{ kPa}$, $\dot{V}_{\text{in}} = 100 \cdot 10^3 \frac{\text{m}^3}{\text{h}}$, $\dot{V}_1^L = 61.5 \cdot 10^3 \frac{\text{m}^3}{\text{h}}$, $\dot{V}_1^U = 100 \cdot 10^3 \frac{\text{m}^3}{\text{h}}$, $\dot{V}_2^L = 25.3 \cdot 10^3 \frac{\text{m}^3}{\text{h}}$ and $\dot{V}_2^U = 44.4 \cdot 10^3 \frac{\text{m}^3}{\text{h}}$. Further, $\dot{V}_1 = \dot{V}_{\text{in}} \cdot x$ and $\dot{V}_2 = \dot{V}_{\text{in}} \cdot (1-x)$ are explicit functions of x . The functions $w_{1,\text{MLP}}$ and $w_{2,\text{MLP}}$ describe the specific power predicted by the MLPs. The lower and upper bounds of the volumetric flow rates, \dot{V}_1^L , \dot{V}_2^L and \dot{V}_1^U , \dot{V}_2^U correspond to the surge and choke lines of the compressors at the specified pressure ratio of 4.5 (left and right hand boundaries in Figure 4).

The optimization problem (3) is solved using an absolute optimality gap of 10^{-4} and a relative optimality gap of 10^{-12} . Further, a CPU time limit of

100,000 seconds is set. As shown in Table 3, the RS formulation reduces the number of variables from 97 to 1 and eliminates all 96 equality constraints compared to the FS formulation. The RS formulation is solved using the presented solver within 0.23 seconds when using the envelopes. This is over four hundred thousand times faster than the solution with the same solver and relaxation in the FS formulation. BARON converges only using reformulation F_2 (within 25.02 second). When the other reformulations are used, the desired tolerance is not reached within 100,000 seconds. Thus, the proposed approach is over one hundred times faster than BARON if BARON uses F_2 and over four hundred thousand times faster if BARON uses F_1 , F_3 or F_4 .

Table 3: Numerical results of the compressor plant optimization (Subsection 5.3)

	Problem size	Solver	CPU time [s]	Iterations	Abs. gap
(FS)	97 variables	BARON (F_1)	100,000.00	1,934,517	$> 3 \cdot 10^8$
	96 equalities	BARON (F_2)	25.02	892	$< \epsilon_{\text{tol}}$
	4 inequalities	BARON (F_3)	100,000.00	4,224,962	0.6
		BARON (F_4)	100,000.00	3,128,979	0.8
		Presented solver (F_1)			–variable overflow–
		Presented solver (F_2)			–variable overflow–
		Presented solver (F_3)			–variable overflow–
		Presented solver (F_4)			–variable overflow–
	Presented solver (envelope)	100,000.00	846,124	181.2	
(RS)	1 variables	Presented solver (F_1)			–variable overflow–
	0 equalities	Presented solver (F_2)			–variable overflow–
	4 inequalities	Presented solver (F_3)	0.34	171	$< \epsilon_{\text{tol}}$
		Presented solver (F_4)			–variable overflow–
		Presented solver (envelope)	0.23	81	$< \epsilon_{\text{tol}}$

variable overflow: Crashed due to variable overflow in FILIB++.

The optimal solution of the problem is $P_{\text{total}} = 6.20$ MW with a split ratio of $x = 0.683$ that corresponds to $\dot{V}_1 = 68.28 \frac{\text{m}^3}{\text{h}}$ and $\dot{V}_2 = 31.72 \frac{\text{m}^3}{\text{h}}$. The optimization using learned compressor maps can have some advantage over simple operating heuristics. For instance, if the main air compressor would be operated at its most efficient operating point, the the total power consumption would be 6.2% higher ($P_{\text{total}} = 6.61$ MW) and if the flowrates would be divided according to the maximum volumetric capacity of the compressors, the total power consumption would be 9.3% higher ($P_{\text{total}} = 6.84$ MW).

5.4 Cumene Process

In the third numerical example, the operating point of a cumene process is optimized illustrating a complex industrial unit. As illustrated in Figure 5, the cumene process consists of a plug flow reactor, two rectification columns, one flash, several (integrated) heat exchangers and recycles. A detailed process description including necessary details for model building can be found in [80]. For this work, we optimize a hybrid model consisting of 14 MLPs that emulate the process. This hybrid model was provided by Schultz *et al.* [81] who modeled the cumene process in ASPEN Plus and learned the MLPs using simulated data. The optimization problem minimizes the negative total profit P of the process [81]:

$$\begin{aligned}
\min_{\mathbf{x}} \quad & -P = -F_{\text{Prod}} \cdot \$_{\text{Cumpure}} + \text{Fresh}_{\text{C3}} \cdot \$_{\text{C3}} + \text{Fresh}_{\text{benz}} \cdot \$_{\text{benzpure}} \\
& - F_{\text{Gas}} \cdot (Z_{\text{gas}_{\text{benz}}} \cdot \$_{\text{benz}} + Z_{\text{gas}_{\text{cum}}} \cdot \$_{\text{cum}} \\
& + Z_{\text{gas}_{\text{propy}}} \cdot \$_{\text{propy}} + Z_{\text{gas}_{\text{propa}}} \cdot \$_{\text{propa}} \\
& + Z_{\text{gas}_{\text{PBI}}} \cdot \$_{\text{PBI}}) - F_{\text{B2}} \cdot (Z_{\text{B2}_{\text{cum}}} \cdot \$_{\text{cum}} + Z_{\text{B2}_{\text{PBI}}} \cdot \$_{\text{PBI}}) \\
& - Q_{\text{Reactor}} \cdot \$_{\text{Eger}} + (Q_{\text{boiler}} + Q_{\text{rebC1}} + Q_{\text{rebC2}}) \cdot \$_{\text{HP}} \\
& + (Q_{\text{HX1}} + Q_{\text{HX2}}) \cdot \$_{\text{EE}} \\
\text{s.t.} \quad & T_{\text{reactor}} - 390^{\circ}\text{C} \leq 0, \quad 360^{\circ}\text{C} - T_{\text{reactor}} \leq 0, \\
& Q_{\text{rebC1}} - 1.97\text{Gcal/h} \leq 0, \quad 1.31\text{Gcal/h} - Q_{\text{rebC1}} \leq 0, \\
& RR_{\text{C1}} - 1 \leq 0, \quad 0.37 - RR_{\text{C1}} \leq 0, \\
& DF_{\text{C2}} - 0.99 \leq 0, \quad 0.85 - DF_{\text{C2}} \leq 0, \\
& RR_{\text{C2}} - 1.2 \leq 0, \quad 0.2 - RR_{\text{C2}} \leq 0, \\
& 0.999 - Z_{\text{prod}_{\text{cum}}} \leq 0
\end{aligned} \tag{4}$$

with $\mathbf{x} = (T_{\text{reactor}}, Q_{\text{rebC1}}, RR_{\text{C1}}, DF_{\text{C2}}, RR_{\text{C2}})$. A list of all economic parameters ($\$_i$) of the optimization problem can be found in [81].

The hybrid model is composed by 14 MLPs, each consisting 10 to 20 neurons, resulting in a FS optimization problem with 794 variables, 789 equality

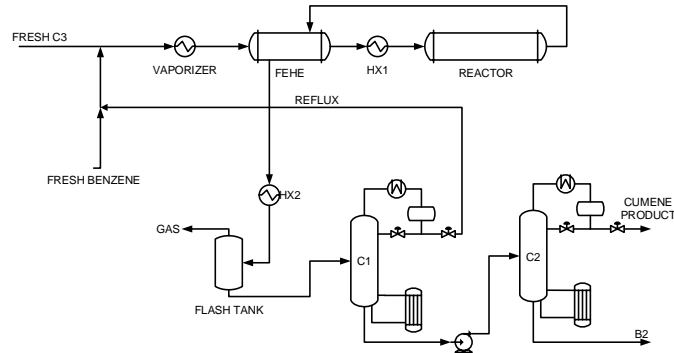


Fig. 5: Graphical illustration of the cumene process

and 1 inequality constraints. The RS formulation constitutes only 5 variables, 0 equality and 1 inequality constraints. Due to the complexity of the case study, the problem is only implemented in the FS formulation in BARON and the RS formulation in the presented solver. The FS formulation in the presented solver is omitted as it is always outperformed by the RS formulation in the previous examples.

Table 4: Numerical results of the cumene process optimization problem (Subsection 5.4)

	Problem size	Solver	CPU time [s]	Iterations	Abs. gap
(FS)	794 variables	BARON (F_1)	100,000.00	110,453	$1 \cdot 10^{20}$
	789 equalities	BARON (F_2)	100,000.00	120,536	$1 \cdot 10^{20}$
	1 inequalities	BARON (F_3)	100,000.00	136,645	$1 \cdot 10^{20}$
		BARON (F_4)	100,000.00	117,400	$1 \cdot 10^{20}$
(RS)	5 variables	Presented solver (F_1)		–variable overflow–	
	0 equalities	Presented solver (F_2)		–variable overflow–	
	1 inequalities	Presented solver (F_3)	100,000.00	4,772,133	$1 \cdot 10^{11}$
		Presented solver (F_4)			–variable overflow–
		Presented solver (envelope)	100,000.00	5,683,103	$8 \cdot 10^{10}$
	Presented solver (envelope)*	100,000.00	12,939,508	$1 \cdot 10^5$	

variable overflow: Crashed due to variable overflow in FILIB++.

*: Adapted setting such that upper bound is obtained by function evaluation, not local search.

The results in Table 4 show that none of the tested solution approaches converge to the desired tolerance within the CPU time limit. In order to analyze this, a convergence plot is provided in Figure 6 that depicts the lower bounds of the solvers over CPU time. Apparently, BARON does not improve its initial lower bound on the objective at all. In comparison, the presented solver

improves its lower bound steadily but slowly. Due to the high complexity of the case-study another optimization run (annotated with the asterisk (*)) is executed using adapted solver options. More precisely, instead of using a local NLP solver in each iteration for upper bounding, the objective function is just evaluated at the center of the current interval. This leads to about 2.3 times more iterations in the same CPU time and further improvements of the lower bound. However, the complex example would still require longer CPU times to converge to the desired tolerance.

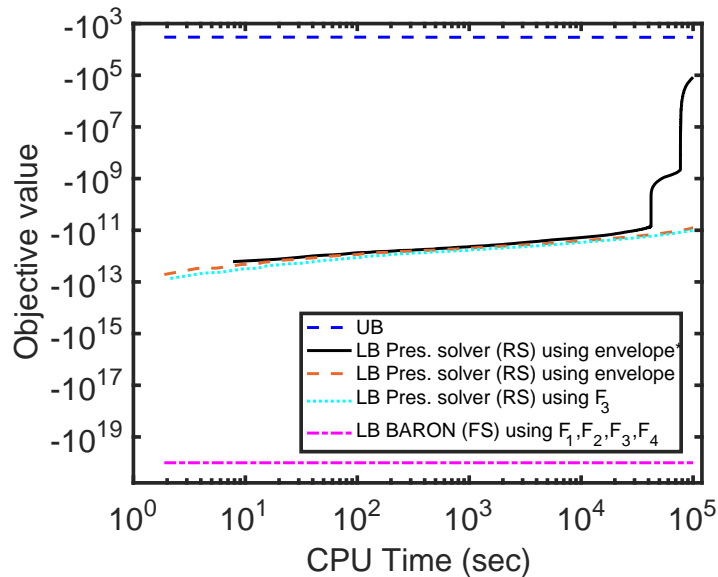


Fig. 6: Convergence plot of the cumene process optimization problem (Subsection 5.4). Herein, UB refers to the upper bound and LB to the lower bound of the corresponding solvers. The asterisk (*) refers to adapted solver options such that the upper bound is obtained by function evaluation, not local search

6 Conclusion and Future Work

A method for deterministic global optimization of ANN embedded optimization problems is presented. The proposed method formulates the problem in a RS and computes lower bounds by propagation of McCormick relaxations through the network equations. Thus, variables inside the ANNs and the network equa-

tions are not visible to the optimization algorithm and problem size is reduced significantly.

The proposed method is tested on four numerical examples including one illustrative function and three engineering applications. In all examples, the number of optimization variables and equality constraints could be reduced by the RS formulations. In particular, problems including ANNs with a large number of neurons benefit from the RS formulation. Further, the RS formulation results in all examples in an acceleration of the optimization by factors of up to four hundred thousand compared to the FS formulation using the same solver. A direct comparison to the state-of-the-art solver BARON, which works in FS, is more difficult because BARON currently does not include the hyperbolic tangent activation function. However, the results suggest that the combination of the RS formulation and the envelopes yield favorable performance of the proposed method in comparison to BARON.

In terms of problem sizes, the proposed approach optimized single shallow ANNs with up to 700 neurons in under 10 seconds. An analysis of the scaling of the approach also reveals that deep networks require more CPU time for optimization than shallow networks with the same or even larger number of neurons. Thus, we conclude that shallow ANNs are currently more suitable for efficient optimization than deep ANNs. The engineering examples further embed up to 14 ANNs. Although, two of the engineering applications could be solved within a fraction of a second, the solution of the complex cumene process case-study converges slowly. This is probably due to the propagation of relaxations through a large number of ANNs and equations. In general, the considered problem sizes significantly exceed the examples for deterministic ANN embedded optimization found in the literature (i.e., Smith *et al.* (2013) [18] optimized an ANN with 1 layer, 3 neurons and 5 inputs using BARON).

As shown in the case studies, the combination of ANNs as universal approximators and an efficient deterministic global optimization algorithm is a powerful tool for various applications. In addition, this method can be further extended

to, for instance, mixed integer problems where a process superstructure is optimized globally [16, 82]. Here, unit operations, thermodynamic models and even dynamics could be emulated by ANNs allowing the utilization of data from different sources such as experiments, process simulations and life-cycle assessment tools (e.g., [83]). Also, complex model parts could be replaced by ANNs that lump these complex parts yielding possibly tight relaxations and less optimization variables. Other possible extension of the proposed method could be more efficient methods for optimization of deep ANNs with a large number of neurons as well as deterministic global training of ANNs.

7 Acknowledgements

The authors gratefully acknowledge the financial support of the Kopernikus-project SynErgie by the Federal Ministry of Education and Research (BMBF) and the project supervision by the project management organization Projektträger Jülich (PtJ). We are grateful to Jaromil Najam, Dominik Bongartz and Susanne Scholl for their work on MAiNGO and Benoît Chachuat for providing MC++. We thank Eduardo Schutz for providing the model of the fourth numerical example, Adrian Caspari & Pascal Schäfer for helpful discussions and Linus Netze & Nils Graß for implementing case studies.

A Appendix

A.1 Convex and Concave Envelopes of the Hyperbolic Tangent Activation Function

In this subsection, the envelopes of the hyperbolic tangent (\tanh) function are derived on a compact interval $D = [x^L, x^U]$. As the hyperbolic tangent function is one-dimensional, McCormick [50] gives a method to construct its envelopes. More specifically, as the hyperbolic tangent function is convex on $(-\infty, 0]$ and concave on $[0, +\infty)$, its convex envelope, $F^{cv} : \mathbb{R} \rightarrow \mathbb{R}$, and concave envelope,

$F^{cc} : \mathbb{R} \rightarrow \mathbb{R}$, are given:

$$F^{cv}(x) = \begin{cases} \tanh(x), & x^U \leq 0 \\ \sec(x), & 0 \leq x^L \\ F_3^{cv}(x), & \text{otherwise} \end{cases} \quad (5)$$

$$F^{cc}(x) = \begin{cases} \sec(x), & x^U \leq 0 \\ \tanh(x), & 0 \leq x^L \\ F_3^{cc}(x), & \text{otherwise} \end{cases} \quad (6)$$

where the secant given as $\sec(x) = \frac{\tanh(x^U) - \tanh(x^L)}{x^U - x^L}x + \frac{x^U \tanh(x^L) - x^L \tanh(x^U)}{x^U - x^L}$.

For $x^L < 0 < x^U$, the hyperbolic tangent function is nonconvex and nonconcave.

The convex envelope, $F_3^{cv} : \mathbb{R} \rightarrow \mathbb{R}$, for this case is:

$$F_3^{cv}(x) = \begin{cases} \tanh(x), & x \leq x_c^u \\ \frac{\tanh(x^U) - \tanh(x_c^u)}{x^U - x_c^u} \cdot (x - x_c^u) + \tanh(x_c^u), & x > x_c^u \end{cases} \quad (7)$$

where $x_c^u = \max(x_c^{u*}, x^L)$ and x_c^{u*} is the solution of:

$$1 - \tanh^2(x_c^u) = \frac{\tanh(x^U) - \tanh(x_c^u)}{x^U - x_c^u}, \quad x_c^u \leq 0 \quad (8)$$

solved numerically for every interval. Similarly, the concave envelope, $F_3^{cc} : \mathbb{R} \rightarrow$

\mathbb{R} , of \tanh is obtained for $x^L < 0 < x^U$ as:

$$F_3^{cc}(x) = \begin{cases} \frac{\tanh(x_c^o) - \tanh(x^L)}{x_c^o - x^L} \cdot (x - x^L) + \tanh(x^L), & x < x_c^o \\ \tanh(x), & x \geq x_c^o \end{cases} \quad (9)$$

where $x_c^o = \min(x_c^{o*}, x^U)$ and x_c^{o*} is the solution of:

$$1 - \tanh^2(x_c^o) = \frac{\tanh(x_c^o) - \tanh(x^L)}{x_c^o - x^L}, \quad x_c^o \geq 0 \quad (10)$$

In the following, we show that the convex and concave envelopes of the hyperbolic tangent function are smooth (C^1) and strictly monotonically increasing.

Proposition A.1 (*smoothness of hyperbolic tangent relaxations*). *The convex and concave envelopes of the hyperbolic tangent function, $F^{cv}(x)$ and F^{cc} , are once continuously differentiable (C^1) and in general not C^2 .*

Proof For $x^U \leq 0$, $F^{cv}(x) = \tanh(x)$ and $F^{cc}(x) = \sec(x)$ which are C^∞ . Similarly, for $0 \leq x^L$, $F^{cc}(x) = \tanh(x)$ and $F^{cv}(x) = \sec(x)$ which are C^∞ . For $x^L < 0 < x^U$, the envelopes are given by (7) and (9). These are at least once continuously differentiable (C^1) because of (8) and (10). (7) and (9) are at most C^1 because

$$\left. \frac{d^2(F_3^{cv})}{dx^2} \right|_x = \begin{cases} -2 \operatorname{sech}^2(x) \tanh(x), & x < x_c^u \\ 0, & x \geq x_c^u \end{cases} \quad (11)$$

and

$$\left. \frac{d^2(F_3^{cc})}{dx^2} \right|_x = \begin{cases} 0, & x < x_c^o \\ -2 \operatorname{sech}^2(x) \tanh(x), & x \geq x_c^o \end{cases} \quad (12)$$

where $\operatorname{sech}(x)$ is the hyperbolic secant function, are not continuous at x_c^u and x_c^o , respectively. \square As shown in Proof A.1, the

first derivative of the convex and concave envelopes of the hyperbolic tangent function, $\frac{d(F^{cv})}{dx}$ and $\frac{d(F^{cc})}{dx}$, are continuous but not continuously differentiable.

The following proof shows that the first derivative of the convex and concave envelopes of the hyperbolic tangent function are Lipschitz continuous.

Proposition A.2 (*Lipschitz continuity of 1st derivative of hyperbolic tangent relaxations*). *The second derivative of the convex and concave envelopes of the hyperbolic tangent function are bounded. This implies that the first derivative of the convex and concave envelopes of the hyperbolic tangent function, $\frac{d(F_3^{cv})}{dx}$ and $\frac{d(F_3^{cc})}{dx}$, are at least once Lipschitz continuous.*

Proof For $x^U \leq 0$, $F^{cv}(x) = \tanh(x)$ and $F^{cc}(x) = \sec(x)$ which are C^∞ . Similarly, for $0 \leq x^L$, $F^{cc}(x) = \tanh(x)$ and $F^{cv}(x) = \sec(x)$ which are C^∞ . For $x^L < 0 < x^U$, the second derivative of the convex and concave envelopes of the hyperbolic tangent function are given by (11) and (12). This implies that

$$\left| \frac{d^2(F_3^{cv}(x))}{dx^2} \right| \leq 2 |\operatorname{sech}^2(\tilde{x}^{cv}) \tanh(\tilde{x}^{cv})| = 2 \left| \frac{\sinh(\tilde{x}^{cv})}{\cosh^3(\tilde{x}^{cv})} \right| \quad (13)$$

with $x^L \leq x \leq x^U$ and $x^L \leq \tilde{x}^{cv} \leq x_c^u$. From $\cosh(x) \geq 1$ it follows that

$$2 \left| \frac{\sinh(\tilde{x}^{cv})}{\cosh^3(\tilde{x}^{cv})} \right| \leq 2 |\sinh(\tilde{x}^{cv})| \quad (14)$$

As $\sinh(x)$ is a monotonic function that is point symmetric with respect to the origin and $x^L \leq \tilde{x}^{cv} \leq 0$, it follows that the second derivative of the convey envelope is bounded

$$2 |\sinh(\tilde{x}^{cv})| \leq 2 \sinh(|x^L|) \quad (15)$$

Thus, the first derivative of the convex envelope of the hyperbolic tangent function, $\frac{d(F^{cv})}{dx}$, is at least once Lipschitz continuous with a Lipschitz constant of at most $L^{cv} = 2 \sinh(|x^L|)$.

Similarly, it holds that

$$\left| \frac{d^2(F_3^{cc}(x))}{dx^2} \right| \leq 2 |\operatorname{sech}^2(\tilde{x}^{cc}) \tanh(\tilde{x}^{cc})| \leq 2 |\sinh(\tilde{x}^{cc})| \quad (16)$$

with $x^L \leq x \leq x^U$ and $0 \leq x_c^o \leq \tilde{x}^{cc} \leq x^U$. It follows that, the first derivative of the concave envelope of the hyperbolic tangent function, $\frac{d(F^{cc})}{dx}$, is at least once Lipschitz continuous with a Lipschitz constant of at most $L^{cc} = 2 \sinh(|x^U|)$. \square

Proposition A.3 (*monotonicity of hyperbolic tangent relaxations*). *The convex and concave envelopes of the hyperbolic tangent function are strictly monotonically increasing.*

Proof For $x^U \leq 0$, $F^{cv}(x) = \tanh(x)$ and $F^{cc}(x) = \sec(x)$. Similarly, for $0 \leq x^L$, $F^{cc}(x) = \tanh(x)$ and $F^{cv}(x) = \sec(x)$. As $\frac{d(\tanh(x))}{dx} = 1 - \tanh^2(x) >$

0, $\tanh(x)$ is strictly monotonic monotonically. As $x^U > x^L$, $\sec(x)$ is strictly monotonically increasing. For $x^L < 0 < x^U$, the envelopes are given by (7) and (9). These are again strictly monotonically increasing because $x_c^o > x^L$ and $x^U > x_c^u$. \square

A.2 Convex and Concave Envelopes of the Sigmoid Activation Function

Another common activation function of ANNs is the sigmoid function. The sigmoid function can be reformulated using $\text{sig}(x) = \frac{1}{2}(1 + \tanh(\frac{x}{2}))$. The convex and concave envelopes of the sigmoid function, $F_{\text{sig}}^{cv}(x)$ and $F_{\text{sig}}^{cc}(x)$, can be derived using the reformulation and the convex and concave envelopes of the hyperbolic tangent function, $F_{\tanh}^{cv}(x)$ and $F_{\tanh}^{cc}(x)$:

$$F_{\text{sig}}^{cv}(x) = \frac{1}{2} \left(1 + F_{\tanh}^{cv}\left(\frac{x}{2}\right) \right) \quad (17)$$

$$F_{\text{sig}}^{cc}(x) = \frac{1}{2} \left(1 + F_{\tanh}^{cc}\left(\frac{x}{2}\right) \right) \quad (18)$$

For simplicity, this manuscript does not provide proofs for smoothness and monotonicity of the envelopes of the sigmoid function. However, similar results to the ones for the hyperbolic tangent activation function (see Appendix A.2) can be derived for the sigmoid activation function.

A.3 McCormick Relaxations of Reformulations of the Hyperbolic Tangent Activation Function

Reformulations of the hyperbolic tangent function are necessary for solvers where the hyperbolic tangent function is not directly available. Four common reformulations $F_1, F_2, F_3, F_4 : \mathbb{R} \rightarrow \mathbb{R}$ are defined as follows:

$$F_1(x) := \frac{e^x - e^{-x}}{e^x + e^{-x}} = \tanh(x) \quad (19)$$

$$F_2(x) := \frac{e^{2x} - 1}{e^{2x} + 1} = \tanh(x) \quad (20)$$

$$F_3(x) := 1 - \frac{2}{e^{2x} + 1} = \tanh(x) \quad (21)$$

$$F_4(x) := \frac{1 - e^{-2x}}{1 + e^{-2x}} = \tanh(x) \quad (22)$$

The convex and concave relaxations of F_1, F_2, F_3, F_4 can be computed using MC++. It can be shown that the convex and concave relaxations of F_1, F_2 and F_4 are weaker than the ones of F_3 in specific cases (e.g., on the interval $x \in D = [-1, 1]$). Further, the convex and concave relaxations of F_1, F_2 and F_4 are not differentiable. Finally, it can be observed that relaxations of the reformulations are considerably weaker than the envelopes of the hyperbolic tangent function.

References

- [1] Hornik, K., Stinchcombe, M., White, H.: Multilayer feedforward networks are universal approximators. *Neural Networks* **2**(5), 359–366 (1989). DOI 10.1016/0893-6080(89)90020-8
- [2] Gasteiger, J., Zupan, J.: Neural networks in chemistry. *Angewandte Chemie International Edition in English* **32**(4), 503–527 (1993). DOI 10.1002/anie.199305031
- [3] Azlan Hussain, M.: Review of the applications of neural networks in chemical process control - simulation and online implementation. *Artificial Intelligence in Engineering* **13**(1), 55–68 (1999). DOI 10.1016/S0954-1810(98)00011-9
- [4] Agatonovic-Kustrin, S., Beresford, R.: Basic concepts of artificial neural network modeling and its application in pharmaceutical research. *Journal*

- of Pharmaceutical and Biomedical Analysis **22**(5), 717–727 (2000). DOI 10.1016/S0731-7085(99)00272-1
- [5] Witek-Krowiak, A., Chojnacka, K., Podstawczyk, D., Dawiec, A., Pokomeda, K.: Application of response surface methodology and artificial neural network methods in modelling and optimization of biosorption process. *Bioresource technology* **160**, 150–160 (2014). DOI 10.1016/j.biortech.2014.01.021
- [6] Meireles, M., Almeida, P., Simoes, M.G.: A comprehensive review for industrial applicability of artificial neural networks. *IEEE Transactions on Industrial Electronics* **50**(3), 585–601 (2003). DOI 10.1109/TIE.2003.812470
- [7] Del Rio-Chanona, E.A., Fiorelli, F., Zhang, D., Ahmed, N.R., Jing, K., Shah, N.: An efficient model construction strategy to simulate microalgal lutein photo-production dynamic process. *Biotechnology and Bioengineering* **114**(11), 2518–2527 (2017). DOI 10.1002/bit.26373
- [8] Cheema, J.J.S., Sankpal, N.V., Tambe, S.S., Kulkarni, B.D.: Genetic programming assisted stochastic optimization strategies for optimization of glucose to gluconic acid fermentation. *Biotechnology progress* **18**(6), 1356–1365 (2002). DOI 10.1021/bp015509s
- [9] Desai, K.M., Survase, S.A., Saudagar, P.S., Lele, S.S., Singhal, R.S.: Comparison of artificial neural network and response surface methodology in fermentation media optimization: Case study of fermentative production of scleroglucan. *Biochemical Engineering Journal* **41**(3), 266–273 (2008). DOI 10.1016/j.bej.2008.05.009
- [10] Nagata, Y., Chu, K.H.: Optimization of a fermentation medium using neural networks and genetic algorithms. *Biotechnology Letters* **25**(21), 1837–1842 (2003). DOI 10.1023/A:1026225526558
- [11] Fahmi, I., Cremaschi, S.: Process synthesis of biodiesel production plant using artificial neural networks as the surrogate models. *Computers &*

- Chemical Engineering **46**, 105–123 (2012). DOI 10.1016/j.compchemeng.2012.06.006
- [12] Nascimento, C.A.O., Giudici, R., Guardani, R.: Neural network based approach for optimization of industrial chemical processes. *Computers & Chemical Engineering* **24**(9-10), 2303–2314 (2000). DOI 10.1016/S0098-1354(00)00587-1
- [13] Nascimento, C.A.O., Giudici, R.: Neural network based approach for optimisation applied to an industrial nylon-6,6 polymerisation process. *Computers & Chemical Engineering* **22**, 595–S600 (1998). DOI 10.1016/S0098-1354(98)00105-7
- [14] Chambers, M., Mount-Campbell, C.A.: Process optimization via neural network metamodeling. *International Journal of Production Economics* **79**(2), 93–100 (2002). DOI 10.1016/S0925-5273(00)00188-2
- [15] Henao, C.A., Maravelias, C.T.: Surrogate-based process synthesis. In: S. Pierucci, G.B. Ferraris (eds.) 20th European Symposium on Computer Aided Process Engineering, *Computer Aided Chemical Engineering*, vol. 28, pp. 1129–1134. Elsevier, Milano, Italy (2010). DOI 10.1016/S1570-7946(10)28189-0
- [16] Henao, C.A., Maravelias, C.T.: Surrogate-based superstructure optimization framework. *AIChE Journal* **57**(5), 1216–1232 (2011). DOI 10.1002/aic.12341
- [17] Sant Anna, H.R., Barreto, A.G., Tavares, F.W., de Souza, M.B.: Machine learning model and optimization of a psa unit for methane-nitrogen separation. *Computers & Chemical Engineering* **104**, 377–391 (2017). DOI 10.1016/j.compchemeng.2017.05.006
- [18] Smith, J.D., Neto, A.A., Cremaschi, S., Crunkleton, D.W.: CFD-based optimization of a flooded bed algae bioreactor. *Industrial & Engineering Chemistry Research* **52**(22), 7181–7188 (2013). DOI 10.1021/ie302478d

- [19] Henao, C.A.: A superstructure modeling framework for process synthesis using surrogate models. Dissertation, University of Wisconsin, Madison (2012)
- [20] Kajero, O.T., Chen, T., Yao, Y., Chuang, Y.C., Wong, D.S.H.: Meta-modelling in chemical process system engineering. *Journal of the Taiwan Institute of Chemical Engineers* **73**, 135–145 (2017). DOI 10.1016/j.jtice.2016.10.042
- [21] Lewandowski, J., Lemcoff, N.O., Palosaari, S.: Use of neural networks in the simulation and optimization of pressure swing adsorption processes. *Chemical Engineering & Technology* **21**(7), 593–597 (1998). DOI 10.1002/(SICI)1521-4125(199807)21:7<593::AID-CEAT593>3.0.CO;2-U
- [22] Gutierrez-Antonio, C.: Multiobjective stochastic optimization of dividing-wall distillation columns using a surrogate model based on neural networks. *Chemical and Biochemical Engineering Quarterly* **29**(4), 491–504 (2016). DOI 10.15255/CABEQ.2014.2132
- [23] Chen, C.R., Ramaswamy, H.S.: Modeling and optimization of variable retort temperature (vrt) thermal processing using coupled neural networks and genetic algorithms. *Journal of Food Engineering* **53**(3), 209–220 (2002). DOI 10.1016/S0260-8774(01)00159-5
- [24] Dornier, M., Decloux, M., Trystram, G., Lebert, A.: Interest of neural networks for the optimization of the crossflow filtration process. *LWT-Food Science and Technology* **28**(3), 300–309 (1995). DOI 10.1016/S0023-6438(95)94364-1
- [25] Fernandes, F.A.N.: Optimization of fischer-tropsch synthesis using neural networks. *Chemical Engineering & Technology* **29**(4), 449–453 (2006). DOI 10.1002/ceat.200500310
- [26] Grossmann, I.E., Viswanathan, J., Vecchiotti, A., Raman, R., Kalvelagen,

- E.: GAMS/DICOPT: A discrete continuous optimization package. GAMS Corporation Inc (2002)
- [27] Drud, A.S.: Conopt - a large-scale grg code. *ORSA Journal on Computing* **6**(2), 207–216 (1994). DOI 10.1287/ijoc.6.2.207
- [28] Nandi, S., Ghosh, S., Tambe, S.S., Kulkarni, B.D.: Artificial neural-network-assisted stochastic process optimization strategies. *AIChE Journal* **47**(1), 126–141 (2001). DOI 10.1002/aic.690470113
- [29] Ryoo, H.S., Sahinidis, N.V.: A branch-and-reduce approach to global optimization. *Journal of Global Optimization* **8**(2), 107–138 (1996). DOI 10.1007/BF00138689
- [30] Tawarmalani, M., Sahinidis, N.V.: Global optimization of mixed-integer nonlinear programs: A theoretical and computational study. *Mathematical Programming* **99**(3), 563–591 (2004). DOI 10.1007/s10107-003-0467-6
- [31] Tawarmalani, M., Sahinidis, N.V.: A polyhedral branch-and-cut approach to global optimization. *Mathematical Programming* **103**(2), 225–249 (2005). DOI 10.1007/s10107-005-0581-8
- [32] Bradford, E., Schweidtmann, A.M., Lapkin, A.A.: Efficient multiobjective optimization employing gaussian processes, spectral sampling and a genetic algorithm. In Revision (2018)
- [33] Forrester, A.I., Keane, A.J.: Recent advances in surrogate-based optimization. *Progress in Aerospace Sciences* **45**(1-3), 50–79 (2009). DOI 10.1016/j.paerosci.2008.11.001
- [34] Jones, D.R.: A taxonomy of global optimization methods based on response surfaces. *Journal of Global Optimization* **21**(4), 345–383 (2001). DOI 10.1023/A:1012771025575
- [35] Sacks, J., Welch, W.J., Mitchell, T.J., Wynn, H.P.: Design and analysis

- of computer experiments. *Statistical science* **4**(4), 409–423 (1989). DOI 10.1214/ss/1177012413
- [36] Shahriari, B., Swersky, K., Wang, Z., Adams, R.P., de Freitas, N.: Taking the human out of the loop: A review of bayesian optimization. *Proceedings of the IEEE* **104**(1), 148–175 (2016). DOI 10.1109/JPROC.2015.2494218
- [37] Schweidtmann, A.M., Holmes, N., Bradford, E., Bourne, R., Lapkin, A.: Multi-objective self-optimization of continuous flow reactors. In preparation (2018)
- [38] Wilson, Z.T., Sahinidis, N.V.: The ALAMO approach to machine learning. *Computers & Chemical Engineering* **106**, 785–795 (2017). DOI 10.1016/j.compchemeng.2017.02.010
- [39] Cozad, A., Sahinidis, N.V., Miller, D.C.: A combined first-principles and data-driven approach to model building. *Computers & Chemical Engineering* **73**, 116–127 (2015). DOI 10.1016/j.compchemeng.2014.11.010
- [40] Cozad, A., Sahinidis, N.V., Miller, D.C.: Learning surrogate models for simulation-based optimization. *AIChE Journal* **60**(6), 2211–2227 (2014). DOI 10.1002/aic.14418
- [41] Falk, J.E., Soland, R.M.: An algorithm for separable nonconvex programming problems. *Management Science* **15**(9), 550–569 (1969). DOI 10.1287/mnsc.15.9.550
- [42] Horst, R., Tuy, H.: *Global Optimization: Deterministic Approaches*, 3 edn. Springer, Berlin, Heidelberg (1996). DOI 10.1007/978-3-662-03199-5
- [43] Misener, R., Floudas, C.A.: ANTIGONE: Algorithms for continuous / integer global optimization of nonlinear equations. *Journal of Global Optimization* **59**(2), 503–526 (2014). DOI 10.1007/s10898-014-0166-2
- [44] Maher, S.J., Fischer, T., Gally, T., Gamrath, G., Gleixner, A., Gottwald, R.L., Hendel, G., Koch, T., Lübbecke, M.E., Miltenberger, M., Mller, B.,

- Pfetsch, M.E., Puchert, C., Rehfeldt, D., Schenker, S., Schwarz, R., Serano, F., Shinano, Y., Weninger, D., Witt, J.T., Witzig, J.: The SCIP optimization suite (version 4.0)
- [45] Epperly, T.G.W., Pistikopoulos, E.N.: A reduced space branch and bound algorithm for global optimization. *Journal of Global Optimization* **11**(3), 287–311 (1997). DOI 10.1023/A:1008212418949
- [46] Mitsos, A., Chachuat, B., Barton, P.I.: McCormick-based relaxations of algorithms. *SIAM Journal on Optimization* **20**(2), 573–601 (2009). DOI 10.1137/080717341
- [47] Scott, J.K., Stuber, M.D., Barton, P.I.: Generalized McCormick relaxations. *Journal of Global Optimization* **51**(4), 569–606 (2011). DOI 10.1007/s10898-011-9664-7
- [48] Bongartz, D., Mitsos, A.: Deterministic global optimization of process flowsheets in a reduced space using McCormick relaxations. *Journal of Global Optimization* **20**(9), 419 (2017). DOI 10.1007/s10898-017-0547-4
- [49] Huster, W.R., Bongartz, D., Mitsos, A.: Deterministic global optimization of the design of a geothermal organic rankine cycle. *Energy Procedia* **129**, 50–57 (2017). DOI 10.1016/j.egypro.2017.09.181
- [50] McCormick, G.P.: Computability of global solutions to factorable nonconvex programs: Part I - convex underestimating problems. *Mathematical Programming* **10**(1), 147–175 (1976). DOI 10.1007/BF01580665
- [51] McCormick, G.P.: *Nonlinear programming: theory, algorithms, and applications*. John Wiley & Sons, Inc (1983)
- [52] Bompadre, A., Mitsos, A.: Convergence rate of McCormick relaxations. *Journal of Global Optimization* **52**(1), 1–28 (2012). DOI 10.1007/s10898-011-9685-2

- [53] Najman, J., Mitsos, A.: Convergence analysis of multivariate McCormick-relaxations. *Journal of Global Optimization* **66**(4), 597–628 (2016). DOI 10.1007/s10898-016-0408-6
- [54] Tsoukalas, A., Mitsos, A.: Multivariate McCormick relaxations. *Journal of Global Optimization* **59**(2-3), 633–662 (2014). DOI 10.1007/s10898-014-0176-0
- [55] Wechsung, A., Barton, P.I.: Global optimization of bounded factorable functions with discontinuities. *Journal of Global Optimization* **58**(1), 1–30 (2014). DOI 10.1007/s10898-013-0060-3
- [56] Khan, K.A., Watson, H.A.J., Barton, P.I.: Differentiable McCormick relaxations. *Journal of Global Optimization* **67**(4), 687–729 (2017). DOI 10.1007/s10898-016-0440-6
- [57] Bongartz, D., Mitsos, A.: Infeasible path global flowsheet optimization using McCormick relaxations. In: A. Espuna (ed.) 27th European Symposium on Computer Aided Process Engineering, *Computer Aided Chemical Engineering*, vol. 40. Elsevier, San Diego (2017). DOI 10.1016/B978-0-444-63965-3.50107-0
- [58] Wechsung, A., Scott, J.K., Watson, H.A.J., Barton, P.I.: Reverse propagation of McCormick relaxations. *Journal of Global Optimization* **63**(1), 1–36 (2015). DOI 10.1007/s10898-015-0303-6
- [59] Stuber, M.D., Scott, J.K., Barton, P.I.: Convex and concave relaxations of implicit functions. *Optimization Methods and Software* **30**(3), 424–460 (2015). DOI 10.1080/10556788.2014.924514
- [60] Smith, E.M., Pantelides, C.C.: Global optimisation of nonconvex minlps. *Computers & Chemical Engineering* **21**, 791–796 (1997). DOI 10.1016/S0098-1354(97)87599-0

- [61] Tawarmalani, M., Sahinidis, N.V., Pardalos, P.: Convexification and Global Optimization in Continuous and Mixed-Integer Nonlinear Programming: Theory, Algorithms, Software, and Applications, *Nonconvex Optimization and Its Applications*, vol. 65. Springer, Boston, MA (2002). DOI 10.1007/978-1-4757-3532-1
- [62] Bishop, C.M.: Pattern recognition and machine learning, 8 edn. Information science and statistics. Springer, New York, NY (2009)
- [63] Moore, R.E., Bierbaum, F.: Methods and applications of interval analysis, 2 edn. SIAM studies in applied mathematics. Soc. for Industrial and Applied Mathematics, Philadelphia (1979). DOI 10.1137/1.9781611970906
- [64] Hofschuster, W., Krmer, W.: FILIB++ interval library (version 3.0.2) (1998)
- [65] Chachuat, B.: MC++ (version 2.0): A toolkit for bounding factorable functions (2014)
- [66] Chachuat, B., Houska, B., Paulen, R., Peri'c, N., Rajyaguru, J., Villanueva, M.E.: Set-theoretic approaches in analysis, estimation and control of nonlinear systems. *IFAC-PapersOnLine* **48**(8), 981–995 (2015). DOI 10.1016/j.ifacol.2015.09.097
- [67] Bertsekas, D.P., Nedic, A., Ozdaglar, A.E.: Convex analysis and optimization, *Athena Scientific optimization and computation series*, vol. 1. Athena Scientific, Belmont, Mass. (2003)
- [68] Bertsekas, D.P.: Convex optimization algorithms, *Optimization and computation series*, vol. 4. Athena Scientific, Belmont, Massachusetts (2015)
- [69] Bongartz, D., Najman, J., Scholl, S., Mitsos, A.: MAiNGO: McCormick based Algorithm for mixed integer Nonlinear Global Optimization. Technical report (2018)
- [70] International Business Machines: IBM ilog CPLEX (version 12.1) (2009)

- [71] Gleixner, A.M., Berthold, T., Mller, B., Weltge, S.: Three enhancements for optimization-based bound tightening. *Journal of Global Optimization* **67**(4), 731–757 (2017). DOI 10.1007/s10898-016-0450-4
- [72] Ryoo, H.S., Sahinidis, N.V.: Global optimization of nonconvex NLPs and MINLPs with applications in process design. *Computers & Chemical Engineering* **19**(5), 551–566 (1995). DOI 10.1016/0098-1354(94)00097-2
- [73] Locatelli, M., Schoen, F. (eds.): *Global optimization: Theory, algorithms, and applications*. MOS-SIAM series on optimization. Mathematical Programming Society, Philadelphia, Pa. (2013)
- [74] Kraft, D.: *A Software Package for Sequential Quadratic Programming*. Deutsche Forschungs- und Versuchsanstalt fr Luft- und Raumfahrt Köln: Forschungsbericht. Wiss. Berichtswesen d. DFVLR, Köln (1988)
- [75] Kraft, D.: Algorithm 733: Tomp-fortran modules for optimal control calculations. *ACM Transactions on Mathematical Software* **20**(3), 262–281 (1994). DOI 10.1145/192115.192124
- [76] Johnson, S.G.: *The NLOpt nonlinear-optimization package (version 2.4.2)* (2016)
- [77] Bendtsen, C., Stauning, O.: *Fadbad++ (version 2.1): a flexible C++ package for automatic differentiation* (2012)
- [78] Najman, J., Mitsos, A.: Tighter McCormick relaxations through subgradient propagation. In Revision <https://arxiv.org/abs/1710.09188> (2017)
- [79] Ghorbanian, K., Gholamrezaei, M.: An artificial neural network approach to compressor performance prediction. *Applied Energy* **86**(7-8), 1210–1221 (2009). DOI 10.1016/j.apenergy.2008.06.006
- [80] Luyben, W.L.: Design and control of the cumene process. *Industrial & Engineering Chemistry Research* **49**(2), 719–734 (2010). DOI 10.1021/ie9011535

- [81] Schultz, E.S., Trierweiler, J.O., Farenzena, M.: The importance of nominal operating point selection in self-optimizing control. *Industrial & Engineering Chemistry Research* **55**(27), 7381–7393 (2016). DOI 10.1021/acs.iecr.5b02044
- [82] Lee, U., Burre, J., Caspari, A., Kleinekorte, J., Schweidtmann, A.M., Mitsos, A.: Techno-economic optimization of a green-field post-combustion CO₂ capture process using superstructure and rate-based models. *Industrial & Engineering Chemistry Research* **55**(46), 12,014–12,026 (2016). DOI 10.1021/acs.iecr.6b01668
- [83] Helmdach, D., Yaseneva, P., Heer, P.K., Schweidtmann, A.M., Lapkin, A.A.: A multiobjective optimization including results of life cycle assessment in developing biorenewables-based processes. *ChemSusChem* **10**(18), 3632–3643 (2017). DOI 10.1002/cssc.201700927